Progress of Theoretical Physics, Vol.66, No.6, December 1981

General Relativistic Collapse of Rotating Supermassive Stars

Takashi NAKAMURA and Humitaka SATO

Research Institute for Fundamental Physics
Kyoto University, Kyoto 606

(Received May 25, 1981)

Numerical calculations have been done for the formation process of axisymmetric, rotating supermassive black holes. Polytropic distribution with $N=3$ is used as the initial density distribution. Calculated models are characterized by the total angular momentum (J) and the rotation law. The two types of the initial rotation law are examined. As the effect of rotation is the strongest at the center for the differential rotation law case, the matter distribution becomes disk-like. In this case, if $q=(J/M^2)\lesssim 0.92$ an apparent horizon is formed. If $q\gtrsim 0.92$, the disk-like matter expands toward the lateral direction. For the almost rigidly rotating case, the oblate shape core is always formed because the effect of rotation at the center is not so strong as the former case. In this case if $q\lesssim 1.05$ an apparent horizon is formed. For large q, for example $q=1.46$, the central core bounces and a jet which expands mainly along the rotational axis appears. For the collapse of $10^9 M_\odot$ star, the kinetic energy of the jet becomes 3.6×10^{60} ergs, which is comparable to the total energy stored in the radio lobes of the extra-galactic double radio sources.

§ 1. Introduction

High spatial and spectral resolution observations of NeII (12.8 μm) emission by Lacy et al.[1] showed that there is a mass of $\sim 8\times 10^6 M_\odot$ within the central 1 pc of the Galaxy. Young et al.[2] measured the surface brightness of the peculiar elliptical radio galaxy M87 and concluded that all of the existing data are well fitted by a King model containing a central black hole with $M=5\times 10^9 M_\odot$. Similar observation of NGC6251 by Young et al.[3] showed that there may be a black hole of mass $2.4\times 10^9 M_\odot$ in the central part of NGC6251. These observations strongly suggest that the supermassive black holes do exist in the central part of the galaxies.

As a theoretical model of quasars and active galactic nuclei, Lynden-Bell[4] proposed the accretion disk around the supermassive black hole. This model has been developed by many authors.[5] Spitzer and collaborators[6] proposed the dense stellar system as a model of quasars. Concerning this model, contrary to the suggestion that the collisionally liberated gas condenses into a 'new' main sequence stars, Begelman and Rees[7] have shown that the ultimate fate of the dense stellar cluster is an amorphous supermassive cloud which will eventually collapse or undergo a nuclear explosion. The other important model of quasars is a super-massive star proposed by Hoyle and Fowler.[8] The binding energy of the spheri-

cally symmetric supermassive star ($\sim 10^8 M_\odot$) is very small ($\sim 1 M_\odot c^2$). Such a star begins to collapse by the general relativistic effect for $R \lesssim 3.4 \times 10^{17}$ cm. Rotation and/or magnetic fields are needed to stabilize the supermassive stars. However large rotation causes the rotational instability.[9] After losing the angular momentum, the magnetoids[10] and the spinars[11] will eventually collapse. Thus in all of the models of quasars and active galactic nuclei, there is a phase in which a supermassive cloud, presumably a rotating one, collapses to a black hole or undergoes a nuclear explosion.

The general relativistic collapse of a non-rotating supermassive star was studied by Matsuda and Sato.[12] As for the rotating case, there were the following two works. Wilson[13] has simulated collapses of rotating, magnetized supermassive stars by using a semi-general relativistic code in which the time derivatives of metric tensors are neglected. Fricke[14] has examined the dynamical evolution of rotating supermassive stars using the approximate virial equation. He found gigantic bounces of stars with $M \approx 10^8 M_\odot$ and an energy production up to 10^{60} ergs. However, in this case the minimum radius becomes almost the Schwarzschild one. This means that his approximation is invalid, and a fully general relativistic treatment is needed.

As for the general relativistic collapse of rotating stars, Nakamura et al.[15] proposed a new method including the $[(2+1)+1]$-formalism of the Einstein equations. Using this method, one of the present authors (T.N.)[16] has calculated the general relativistic collapse of rotating stars with $10 M_\odot$ (Paper I). His code is a fully general relativistic 2D code. No approximation other than the finite difference method is used in it. He found that, q being defined by $q =$ [the total angular momentum/(GM_G^2/c)], a black hole is formed if $q \lesssim 0.95$ and it is not if $q \gtrsim 0.95$.

In this paper, we examine the ultimate fate of the collapsing, rotating supermassive stars using the computer code made by one of the authors(T. N.). In § 2, we show the initial conditions and the coordinate conditions. We will show neither the basic equations nor the finite difference method. The former can be found in Paper I. As for the latter, the basic ideas are written in Paper I. The details of the finite difference will be published elsewhere.[17] In § 3, numerical results are shown for various values of q and two types of the rotation law. In § 4, we give a few discussions and astrophysical implications of the numerical results.

§ 2. The initial conditions and the coordinate conditions

We adopt the cylindrical coordinates (R, Z, φ). We assume the system is axially symmetric and is plane symmetric about $Z=0$ plane. In this case full Einstein equations in the $[(2+1)+1]$-formalism can be found in Paper I. We use

$x(=R^2)$ and $y(=Z^2)$ as in Paper I. For simplicity we neglect a nuclear reaction and energy loss by photons and neutrinos. Units of mass, length and time are taken as

$$M=M_B, \qquad L=GM_B/c^2 \quad \text{and} \quad T=GM_B/c^3, \tag{2·1}$$

respectively, where M_B is the total rest mass of baryon.

1) *Initial conditions*

In Paper I, we assumed that there is no poloidal motion at $t=0$. In this paper we take account of the poloidal motion. If we use the conformal approach of O'Murchadha and York,[18] we can easily write down the initial value equations, namely, the constraint equations at $t=0$. As in Paper I, we assume that the initial 3-space metric is conformally flat, that is,

$$\gamma_{ij}=\phi^4(\gamma_{ij})_{\text{flat}}\,. \tag{2·2}$$

The trace and the transverse-traceless part of the extrinsic curvatures are assumed to be zero. Then the extrinsic curvatures (K_{ij}) can be expressed by the 3-space vector (W^R, W^Z, W^φ) as follows:

$$\begin{aligned}
&K_R{}^R=(2/3)(w^R+4x\partial_x w^R-w^Z-2y\partial_y w^Z),\\
&K_Z{}^Z=(2/3)(2w^Z+4y\partial_y w^Z-2w^R-2x\partial_x w^R),\\
&K_\varphi{}^\varphi=(2/3)(w^R-2x\partial_x w^R-w^Z-2y\partial_y w^Z),\\
&k_R{}^Z\equiv K_R{}^Z/R/Z=2(\partial_y w^R+\partial_x w^Z),\\
&K_R{}^\varphi=2R\partial_x W^\varphi
\end{aligned} \tag{2·3}$$

and

$$K_Z{}^\varphi=2Z\partial_y W^\varphi,$$

where

$$w^R=W^R/R \text{ and } w^Z=W^Z/Z.$$

Let ρ_H, J_ϕ, J_R and J_Z be the energy density, the angular momentum density, the momentum density in R-direction and the momentum density in Z-direction measured by the normal line observer whose four velocity is the normal vector to the $t=$constant hypersurface, respectively. The initial value equations become,

a) the Hamiltonian constraint equation,

$$\begin{aligned}
&4(\partial_x\phi+x\partial_{xx}\phi)+2\partial_y\phi+4y\partial_{yy}\phi\\
&\quad=-2\pi(\rho_H\phi^6)\phi^{-1}-\phi^5 x\{x(\partial_x W^\varphi)^2+y(\partial_y W^\varphi)^2\}\\
&\qquad-\frac{1}{8}\phi^5\{(K_R{}^R)^2+(K_Z{}^Z)^2+(K_\varphi{}^\varphi)^2+2xy(k_R{}^Z)^2\},
\end{aligned} \tag{2·4}$$

b) the angular momentum constraint equation,

$$(8+24x\phi^{-1}\partial_x\phi)\partial_x W^{\varphi}+4x\partial_{xx}W^{\varphi}$$
$$+(2+24y\phi^{-1}\partial_y\phi)\partial_y W^{\varphi}+4y\partial_{yy}W^{\varphi}=8\pi J_{\phi}x^{-1}, \tag{2·5}$$

c) the momentum constraint equation,

$$(16x/3)\partial_{xx}w^R+4y\partial_{yy}w^R+(32/3+32x\phi^{-1}\partial_x\phi)\partial_x w^R$$
$$+(2+24y\phi^{-1}\partial_y\phi)\partial_y w^R+8\phi^{-1}\partial_x\phi w^R+(4/3)y\partial_{xy}w^Z$$
$$+(2/3+24y\phi^{-1}\partial_y\phi)\partial_x w^Z-8y\phi^{-1}\partial_x\phi\partial_y w^Z-8\phi^{-1}\partial_x\phi w^Z$$
$$=8\pi J_R/R, \tag{2·6}$$

and

$$4x\partial_{xx}w^Z+(16/3)y\partial_{yy}w^Z+(4+24x\phi^{-1}\partial_x\phi)\partial_x w^Z$$
$$+(8+32y\phi^{-1}\partial_y\phi)\partial_y w^Z+16\phi^{-1}\partial_y\phi w^Z$$
$$+(4/3)x\partial_{xy}w^R-16x\phi^{-1}\partial_y\phi\partial_x w^R+(4/3+24x\phi^{-1}\partial_x\phi)\partial_y w^R$$
$$-16\phi^{-1}\partial_y\phi w^R=8\pi J_Z/Z. \tag{2·7}$$

The method of solving Eqs. (2·4) and (2·5) is shown in Ref. 15). Equations (2·6) and (2·7) can be solved easily by the S.O.R. (Successive Over Relaxation) method.

Let $\rho_3(r)$ and r_0 be the density distribution of $N=3$ polytrope and an initial radius of a star, respectively. We use the following initial conditions:

$$\rho_H\phi^6=\begin{cases}\rho_3(r) & \text{for } r\leqq\rho_3^{-1}(10^{-6}\rho_3(0)),\\ 10^{-6}\rho_3(0) & \text{for } r>\rho_3^{-1}(10^{-6}\rho_3(0)),\end{cases} \tag{2·8}$$

$$J_R/R=J_Z/Z=\begin{cases}\rho_H C_V & \text{for } r\leq r_0,\\ \rho_H C_V\exp(1-(r/r_0)^2) & \text{for } r>r_0,\end{cases} \tag{2·9}$$

and

$$J_{\phi}=x\rho_H\Omega_0\exp(-C_{\varphi}x/r_0^2), \tag{2·10}$$

where C_V, Ω_0 and C_{φ} are the constants which determine the initial infall velocity, the initial central angular velocity and the rotation law (the distribution of the angular momentum), respectively. As we can see from Eq.(2·8), there is a low density envelope outside the star. However, in the actual numerical calculations, the total mass of this envelope is smaller than $10^{-3}\%$ of the total mass of the star. Therefore the contribution of this envelope to the collapse is negligible.

As an equation of state, we use

$$P=(1/3)\rho\varepsilon, \tag{2·11}$$

where P, ρ and ε are the pressure, the proper mass density and the internal energy density per gram, respectively. Initial distribution of ε is taken as

$$\varepsilon = K\rho^{1/3}. \tag{2·12}$$

Now, r_0, C_V, Ω_0, C_φ and K determine the initial conditions uniquely. In all the calculated models, r_0 is 14.5 and C_V is chosen so that the infall velocity at $r=r_0$ becomes the free fall velocity. Instead of Ω_0 and K, we use J and U defined by

$$J = E_{\rm rot}/|E_{\rm grav}| \quad \text{and} \quad U = E_{\rm int}/|E_{\rm grav}|, \tag{2·13}$$

where $E_{\rm rot}$, $E_{\rm int}$ and $E_{\rm grav}$ are the rotational energy, the internal energy and the gravitational energy of the star, respectively. (See Paper I.) We use one more parameter q, which corresponds to $|a|/M$ in a Kerr black hole. q is defined by

$$q = |\text{total angular momentum}|/(GM_G^2/c), \tag{2·14}$$

where M_G is the gravitational mass.

As the rotation laws, we use two C_φ's as

a) Rotation law A; $C_\varphi = 2$,

b) Rotation law B; $C_\varphi = 10$.

In Fig.1, we show the two rotation laws (the solid lines) and $\rho_3(R)$ (the dashed line). We can see that in the rotation law A, the angular frequency (Ω) drops considerably only at very low density region.

2) *Coordinate conditions*

The shift vector is taken to be zero. Therefore the coordinate line agrees with the normal line of $t=$constant hypersurface. As for the lapse function, the maximal slicing condition is used in almost all of the numerical calculations. Some of the models have been re-calculated by using the hypergeometric slicing condition defined in Paper I.

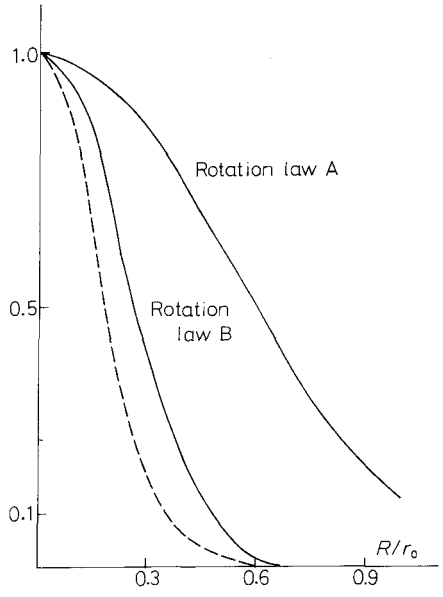

Fig.1. The rotation laws used in the numerical calculation. The solid lines show the distribution of angular frequency (Ω) (defined by $\Omega = \exp(-C_\varphi R^2/r_0^2)$) for two values of C_φ; $C_\varphi = 2$ for the rotation law A and $C_\varphi = 10$ for the rotation law B. The dashed line shows the density distribution of $N=3$ polytrope ($\rho_3(R)$).

§ 3. Numerical results

In Table I, the initial parameters of each model are shown. Since the models are characterized mainly by q and the rotation law, we use them as a name of each model. For example, A146 means the collapse of the rotating supermassive star with $q=1.46$ and the rotation law A. The sixth column (p) in Table I is the ratio of the centrifugal force to the gravitational force at the center. All the calculated models have almost the same internal energy though it is slightly different because ρ_H is given to construct the initial data. The number of grids is 28×28. The coordinate of the outermost grid point is (25,25). In Paper I, some of the models were calculated by using 42×42 grids. However the numerical results have been found to be almost the same as those by 28×28 grids.

1) *Rotation law A*

In this rotation law, the centrifugal force has a maximum value at $R\simeq0.35r_0$ where $\rho_3(R)$ is less than $0.1\rho_3(0)$. (See Fig. 1.) This means if the mass shedding occurs, it will occur from the outer part of the star. In the following, we show the details of the numerical results of the three typical models.

a) Model A 50

Table I. The initial parameters of each model. The name of each model comes from the value of q and the rotation law. For example, A146 means that the collapse of the rotating supermassive star with $q=1.46$ and the rotation law A. The sixth column (p) is the ratio of the centrifugal force to the gravitational force at the center. p is defined by $p=3\Omega_0^2/4\pi\rho\phi^{10}|_{r=0}$. In the seventh column whether an apparent horizon is formed or not is shown.

Model Name	q	U	J	Ω_0	p	Apparent[a] Horizon?
A146	1.46	0.94	0.77	0.32	0.76	NO
A122	1.22	0.86	0.51	0.27	0.50	NO
A105	1.05	0.84	0.37	0.23	0.36	YES
A 93	0.93	0.82	0.29	0.20	0.29	YES
A 75	0.75	0.82	0.19	0.16	0.18	YES
A 50	0.50	0.81	0.08	0.11	0.08	YES
B143	1.43	1.01	1.20	0.76	4.22	NO
B121	1.21	0.88	0.76	0.63	2.86	NO
B104	1.04	0.84	0.54	0.54	2.08	NO
B 92	0.92	0.82	0.42	0.48	1.60	YES[b]
B 74	0.74	0.81	0.27	0.38	1.03	YES[b]
B 51	0.51	0.81	0.12	0.25	0.45	YES

a) The method of determining an apparent horizon is shown in Ref.19).

b) If we use the maximal slicing, no apparent horizon is identified. If we use the hypergeometric slicing defined in Paper I, the apparent horizon is identified. For details see the text.

In this model, the rotation is very slow. At $t=0$, J is 0.08 and the centrifugal force at the center is only 8% of the gravitational force. (See Table I.) At $t=0.287$, the matter distribution is almost spherical and the velocity pattern shows the spherical collapse. (Fig. 2(a)) This feature is kept through the entire time up to when the apparent horizon is formed. (Fig. 2(b)) Although the matter distribu-

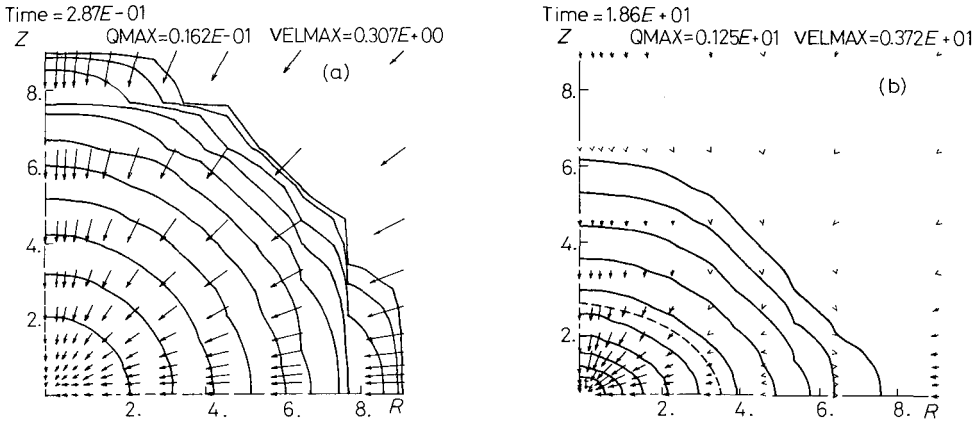

Fig. 2.(a) Contour lines of Q_b at $t=0.287$ for A50. The space integral of Q_b becomes M_B, that is, $2\pi\int_{-\infty}^{\infty}\int_0^{\infty}Q_b R dR dZ = M_B$. The precise definition of Q_b can be found in Paper I. Each line corresponds to $Q_b = \mathrm{QMAX}\cdot 10^{-n/2}$ for $n=1,2,\cdots,11$. QMAX is shown in the figure. Arrows show the vector $(J_R/Q_b, J_Z/Q_b)$. The maximum of this vector is shown in the figure as VELMAX.
(b) The contour lines of Q_b for A50 at $t=18.6$. The notations are the same as Fig. 2(a). The dashed line shows the apparent horizon.

tion becomes slightly oblate by the effect of rotation, all the matter will be swallowed into the slowly rotating black hole.

b) Model A 105

In this model, the star is rather rapidly rotating. At $t=11.5$ (Fig. 3(a)), the matter falls vertically for $R \lesssim 2$. The collapse in the equatorial plane is considerably suppressed by the effect of rotation. For $2.4 \lesssim R \lesssim 7.7$, the outflow velocity reaches up to 0.3c. This outflow is the mass shedding which we expected before. Finally, the oblate shape core is formed in the central region and an apparent horizon is formed outside this core. (Fig. 3(b)) The outer envelope expands along the lateral direction with relativistic velocity. On the $Z=1$ plane the outgoing velocity is 0.34 and 0.70 and the lapse function (α) is 0.82 and 0.88 at $R=5.5$ and 9.1, respectively. If we consider $(1-\alpha)$ as the gravitational potential, we can expect that some part of this envelope will return to the central black hole and the other part will expand to infinity. Thus the ultimate fate of the collapsing supermassive star in this model is completely different from that in

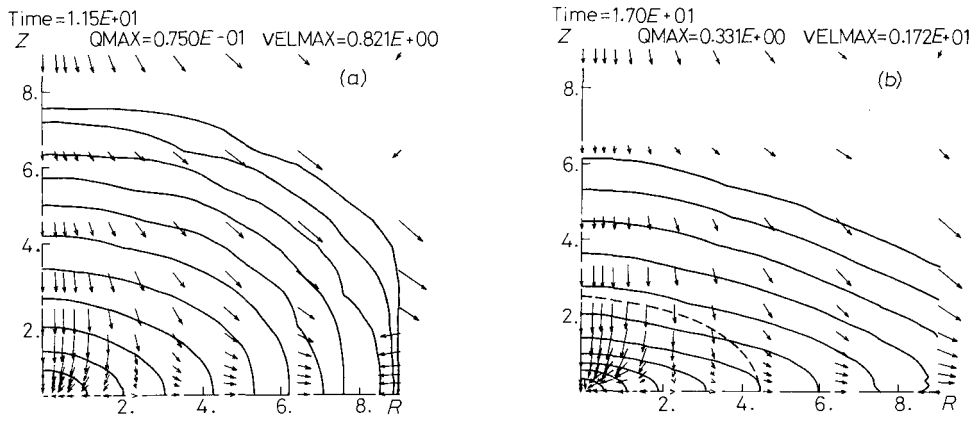

Fig. 3.(a) The contour lines of Q_6 for A105 at $t=11.5$. The notations are the same as Fig. 2(a).
(b) The contour lines of Q_6 for A105 at $t=17.0$. The notations are the same as Fig. 2(b).

Model A50.

c) Model A146

This model is a rapidly rotating case, that is, $J=0.77$ and p is 0.76. At $t=5.76$, the matter in the central part falls almost vertically. For $2\leq R\leq 6.5$, we can see a strong outflow with the velocity up to 0.5. (Fig. 4(a)) At $t=18.8$, the central core bounces and a shock wave is formed. Near the equatorial plane the outflow extends up to $R=9$. The outer thin envelope falls vertically to this outflow and the shock front is formed. (Fig. 4(b)) At $t=23.2$, we can see the strong jet along the rotational axis. The central core has almost stopped moving and the rather dense envelope expands both in the lateral direction and in the Z-direction. (Fig. 4(c)) Finally the strong jet reaches $Z=9$. (Fig. 4(d)) The kinetic and the internal energy of this jet are 2×10^{-3} and 1.5×10^{-3} in our units (Eq.(2·1)), respectively. The total mass of the jet is 5×10^{-3}. Thus the mean kinetic energy per gram of this jet becomes 0.4 (3.6×10^{20} ergs/g). The energy consideration similar to that in A105 shows that this jet will expand to infinity. The total mass and the angular momentum of the relaxed core are 0.21 and 4×10^{-2}, respectively. As the core has a rather small value of $q(\approx1.0)$, it may recollapse eventually and a black hole may be formed after all.

Let us compare the above results with those in Paper I. In Paper I, for slowly rotating cases, the density distribution becomes disk-like and the ring-like singularity appears. However in the present cases of the rotation law A, the density distribution becomes oblate. This difference seems to come from the initial density distribution and the equation of state. As the polytrope with $N=3$ is more centrally condensed type than the exponential distribution in Paper I, the

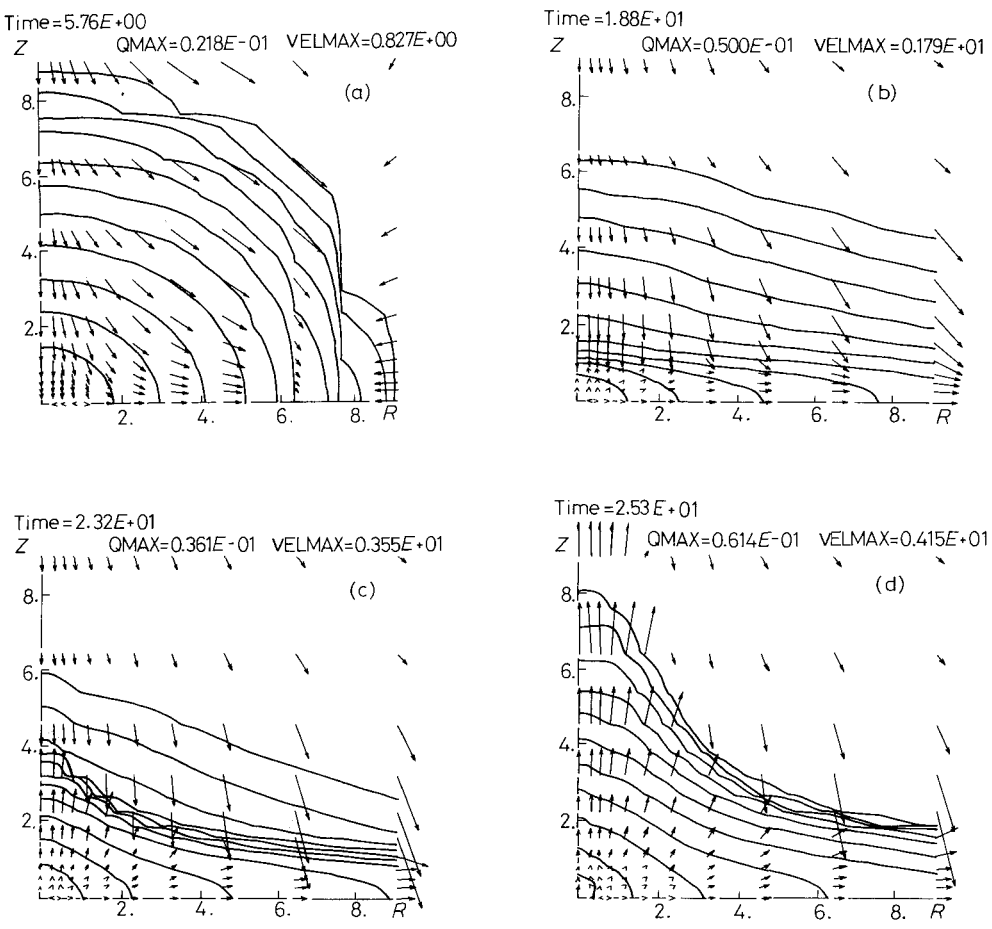

Fig. 4. The contour lines of Q_b for A146 at various time. The notations are the same as Fig. 2(a).

disk will be hardly formed unless the centrifugal force is strong enough in the central region. In Paper I, the equation of state is very hard for $\rho \gtrsim 3\times 10^{14}$ g/cm^3, that is, in the limit of $\rho \to \infty$ the sound velocity becomes the light velocity. Since the equation of state in this paper is very soft, the gravity is stronger than the pressure force and the centrifugal force in the lateral direction for slowly rotating cases.

In Fig. 5, we show the "electric fields" in the [(2+1)+1]-formalism for A105. The strength of the "electric fields" ($|E^4|^2$) does not show a ring-like peak. As the density distribution is not disk-like, the "charge density" (angular momentum density) in the [(2+1)+1]-formalism does not have a ring-like peak contrary to the model M80 in Paper I. (See Fig. 3(b) of Paper I.)

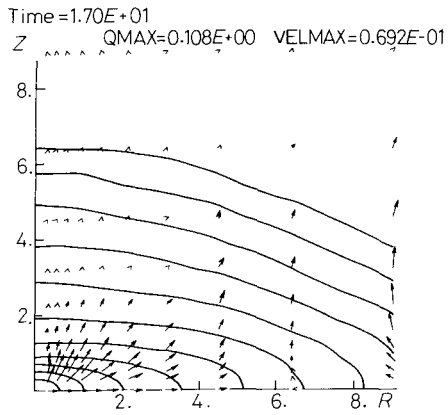

Fig.5. The contour lines of the proper density (ρ) for A105 at $t=17.0$. Each line corresponds to $\rho=\text{QMAX}\times 10^{-n/2}$ for $n=1,2,\cdots,11$. Arrows show the "electric fields" (E^A) in the [(2+1)+1]-formalism. The maximum of $|E^A|$ is shown in the figure as VELMAX.

2) *Rotation law B*

In this rotation law, the centrifugal force is more effective for small R. (See Fig. 1.) This means that, if the mass shedding occurs, it will occur from the central region. In the following, we show the details of the numerical results of the three typical models.

a) Model B51

In Fig. 6, we show the density contours and the flow pattern at $t=21.6$. Although A50 and B51 have almost the same angular momentum, we can see that the central core is deformed rather strongly in B51. Of course, this is due to a rapidly rotating core because of the differential rotation of the rotation law B.

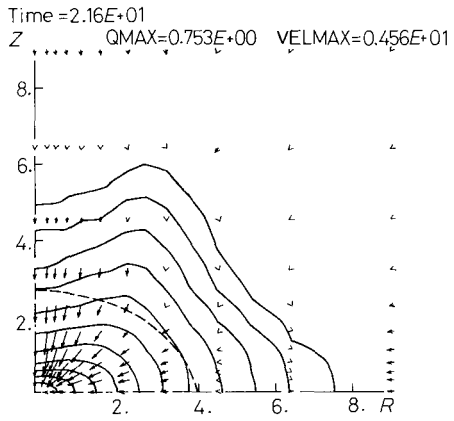

Fig.6. The contour lines of Q_b for B51. The notations are the same as Fig. 2(b).

b) Model B92

In this model, the centrifugal force near the center is greater than the gravitational force at $t=0$ because p is 1.6. This fact causes the outflow of the matter from a small R region. As the rotation is very slow for large R, the matter in the outer part falls almost spherically. (Fig.7(a)) At $t=11.5$, the inflow in the Z-direction and the outflow in the lateral direction form a disk in the central region. (Fig.7(b)) At $t=17.3$, the outgoing velocity of the disk is considerably decelerated. The outer envelope falls into this disk vertically and forms the almost steady shock. For large R, a very thin envelope expands in the

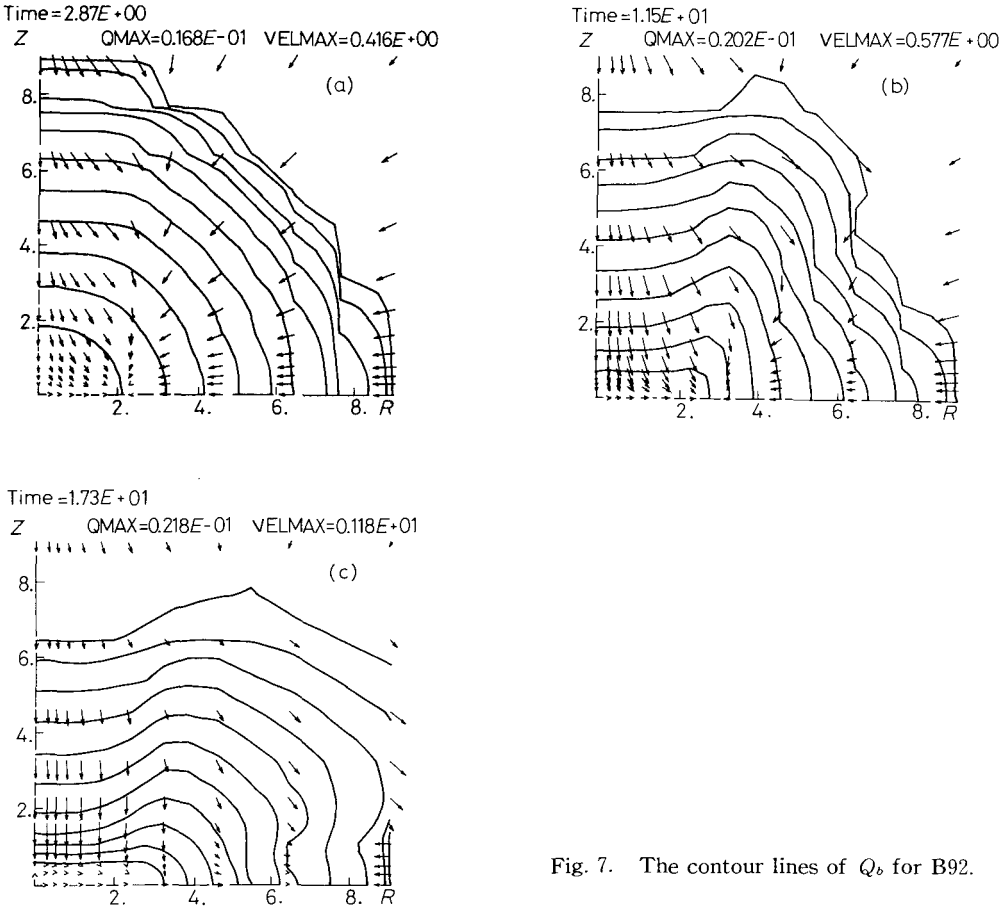

Fig. 7. The contour lines of Q_b for B92.

lateral direction. (Fig. 7(c)) In this model, we have tried to identify an apparent horizon, but in vain. We have recalculated this model using the hypergeometric slicing*) in which the lapse function is spherically symmetric. In this slicing, an apparent horizon is identified. The reason for this difference is the same as that in Paper I. If one uses the maximal slicing as a time slice, the proper time of the co-moving observer, whose four velocity is that of the matter, stops increasing too soon after the density distribution becomes disk-like.

c) Model B143

In this model, we can see the outflow for small R even at rather early time. (Fig. 8(a)) At $t=11.6$, an expanding disk is clearly formed. (Fig. 8(b)) At $t=17.5$, the expansion velocity of the disk is decelerated in the central part and it is the fastest at the edge of the disk. (Fig. 8(c)) At $t=20.8$, the central part of the

*)The definition of the hypergeometric slicing can be found in Paper I.

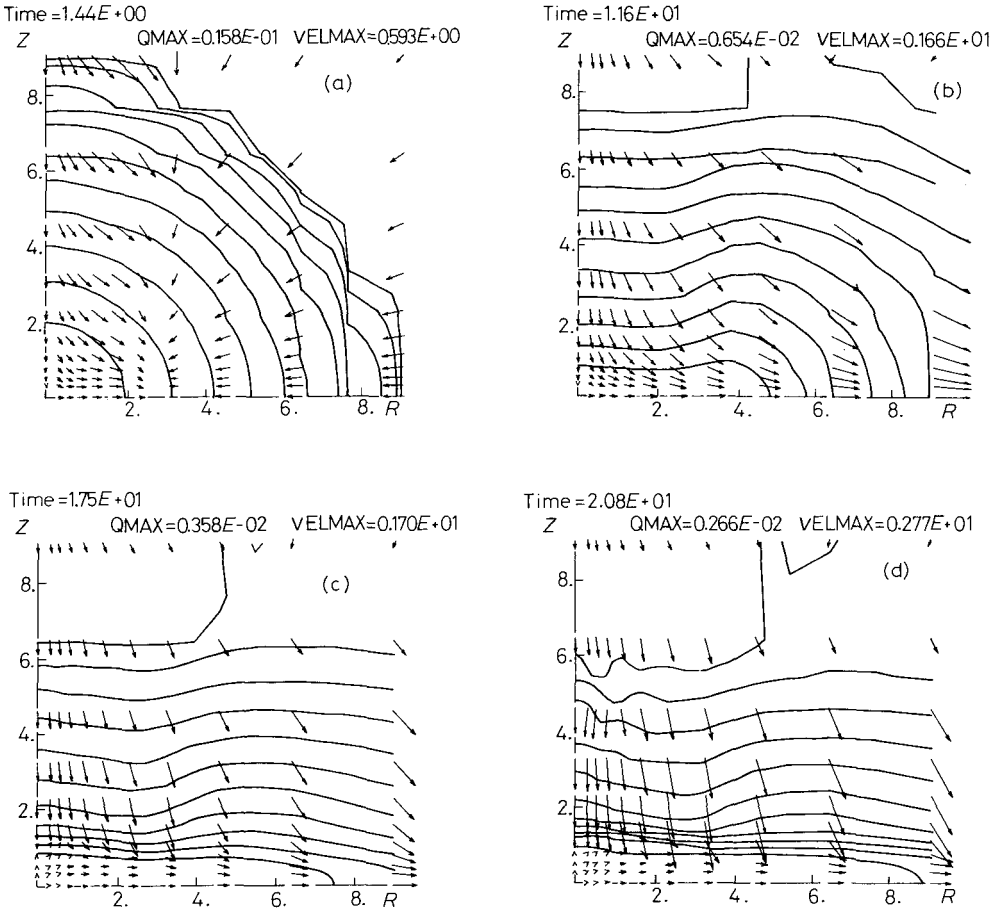

Fig. 8. The contour lines of Q_b for B143.

disk is almost stopped. The outer thin envelope falls into the disk continuously and forms the almost steady shock front. As the expansion velocity is very large in this model, all the matter except the central part will go away from the system. In this model, no jet is formed contrary to the model A146. (Fig. 8(d))

§ 4. Concluding remarks and discussion

In the models using the rotation law A, the apparent horizons are formed for $q \lesssim 1.05$. In the rotation law B, they are formed for $q \lesssim 0.92$. In the models calculated in Paper I, they are formed for $q \lesssim 0.95$. Above three types of the calculated models are different from each other in the equation of state, the initial density distribution, the initial internal energy and the rotation law. However,

it seems that they have almost the same critical value of q for the formation of black holes. In all the models in which the apparent horizon is formed, we have found that peculiar events such as formations of naked singularities do not occur outside the apparent horizon. If we remember that the singularity of the Kerr black hole[20] is hidden by the event horizon for $q<1$, our numerical results of Paper I and this paper suggest that the Kerr black holes may be formed for wide ranges of the initial conditions provided that the density and the angular velocity decrease monotonically with radius. If we take more peculiar initial distributions for density and angular velocity, the singularities might be formed outside the horizon as in the Tomimatsu-Sato metrics.[21]

In the accretion disk model of quasars and active galactic nuclei, the mechanism of the supply of the infalling gas has been unclear although the general infall from the galaxy and/or stellar disruption have been proposed.[22] In the model A105 in this paper, the final result was a rotating black hole plus an expanding envelope. As we have discussed in § 3(1), some part of this expanding envelope is bound to the black hole and the other part not. The former part will return to the system and it may form the accretion disk. If the total mass of this gas is large enough, we do not worry about the gas supply mechanism. It may be possible that the gas left behind at the formation stage of the black holes is the energy source of the quasar activity.

In the model A146, we have seen that the relativistic jet is formed and the central core will recollapse to form a black hole eventually. If we take the total mass of the system, say, $10^9 M_\odot$, which might be the typical value, the kinetic energy and the internal energy of the jet become 3.6×10^{60} ergs and 2.7×10^{60} ergs, respectively. The total mass of the jet is $5\times10^6 M_\odot$. The energy of this jet is comparable to the total energy stored in the radio lobes of the extragalactic double radio sources.[23] In the single explosion model of the double radio sources, the mechanism of the explosion itself has been unclear, although the hydrodynamics after the point explosion have been studied well.[24] The model A146 can be the explosion mechanism of the double radio sources. As we have seen in §3(1), the explosion itself is jet-like contrary to the usual assumption of the spherical explosion. It is now necessary to calculate the expansion of the jets in the ambient gas.

Acknowledgements

The authors would like to thank Professor C. Hayashi for continuous encouragement. This work was supported by the Scientific Research Fund of the Ministry of Education, Science and Culture (564123). One of the authors (T.N) is indebted to Soryushi Shogakukai for the financial aid.

References

1) J. H. Lacy, F. Baas, C. H. Townes and T. R. Geballe, Astrophys. J. **227** (1979), L17.
2) P. J. Young, J. A. Westphal, J. Kristian, C. P. Wilson and F. P. Landauer, Astrophys. J. **221** (1978), 721.
3) P. J. Young, W. L. W. Sargent, J. Kristian and J. A. Westphal, Astrophys. J. **234** (1979), 76.
4) D. Lynden-Bell, Nature **223** (1969), 690.
5) For example;
J. E. Pringle, M. J. Rees and A. G. Pacholczyk, Astron. and Astrophys. **29** (1973), 179.
D. Lynden-Bell and M. J. Rees, Month. Notices Roy. Astron. Soc. **152** (1971), 461.
F. Takahara, Prog. Theor. Phys. **60** (1978), 1606; **62** (1979), 629.
F. Takahara, S. Tsuruta and S. Ichimaru, submitted to Astrophys, J.
6) L. Spitzer and W. C. Saslaw, Astrophys. J. **143** (1966), 400.
L. Spitzer and M. E. Stone, Astrophys. J. **147** (1967), 519.
7) M. C. Begelman and M. J. Rees, Month. Notices. Roy. Astron. Soc. **185** (1978), 847.
8) F. Hoyle and W. A. Fowler, Month. Notices Roy. Astron. Soc. **125** (1963), 169; Nature **197** (1963), 533.
9) W. A. Fowler, "High-Energy Astrophysics" , *Proc, Course 35 Intern. Sch. Phys. "Enrico Fermi"*, ed. L. Gratton (Academic Press, New York, 1966), p. 313.
10) L. M. Ozernoi and V. W. Usov, Ap. and Space Sci. **25** (1973), 531.
11) P. Morrison, Astrophys. J. **157** (1969), L73.
12) T. Matsuda and H. Sato, Prog. Theor. Phys. **41** (1969), 1021.
13) J. Wilson, Varenna Lectures of 1975.
14) K. J. Fricke, Astrophys. J. **189** (1974), 535.
15) T. Nakamura, K. Maeda, S. Miyama and M. Sasaki, Prog. Theor. Phys. **63** (1980), 1229.
K. Maeda, M. Sasaki, T. Nakamura and S. Miyama, Prog. Theor. Phys. **63** (1980), 719.
16) T. Nakamura, Prog. Theor. Phys.**65** (1981), 1876 (Paper I).
17) T. Nakamura, in preparation.
18) N. O'Murchadha and J. W. York, J. Math. Phys. **14** (1973), 1551.
19) M. Sasaki, K. Maeda, S. Miyama and T. Nakamura, Prog. Theor. Phys. **63** (1980), 1051.
20) R. P. Kerr, Phys. Rev. Letters **11** (1963),237.
B. Carter, Phys. Rev. **174** (1968), 1559.
21) A. Tomimatsu and H. Sato, Prog. Theor. Phys. **50** (1973), 95; Phys. Rev. Letters **29** (1972), 1344.
22) M. J. Rees, Physica Scripta **17** (1978), 193.
23) D. S. De Young, Ann. Rev. Astron. Astrophys. **14** (1976), 447.
24) R. H. Sanders, Astrophys. J. **205** (1976), 335.
K. Morita, submitted to Ap. and Space Sci.